Geophysical Research Letters®

Key Points:

- We show clear urban HCHO plumes from 16 cities over the globe by relating satellite pixels with wind fields
- We obtain urban effective HCHO production rates by fitting the downwind structure of HCHO plumes
- Satellite-based effective HCHO production rates provide potential measures of total non-methane volatile organic compound emissions

Supporting Information:

Supporting Information may be found in the online version of this article.

Correspondence to:

L. Zhu,
zhul3@sustech.edu.cn

Observing Downwind Structures of Urban HCHO Plumes From Space: Implications to Non-Methane Volatile Organic Compound Emissions

Xiaoxing Zuo[1] , **Wenfu Sun[2]** , **Isabelle De Smedt[2]** , **Xicheng Li[1]** , **Song Liu[1]** , **Dongchuan Pu[1]** , **Shuai Sun[1]** , **Juan Li[1]** , **Yuyang Chen[1]** , **Weitao Fu[1]**, **Peng Zhang[1]**, **Yali Li[1]**, **Xin Yang[1,3,4]**, **Tzung-May Fu[1,3,4]** , **Huizhong Shen[1,3,4]** , **Jianhuai Ye[1,3,4]** , **Chen Wang[1,3,4]** , and **Lei Zhu[1,3,4]**

[1]School of Environmental Science and Engineering, Southern University of Science and Technology, Shenzhen, China, [2]Division of Atmospheric Reactive Gases, Royal Belgian Institute for Space Aeronomy, Brussels, Belgium, [3]Guangdong Provincial Observation and Research Station for Coastal Atmosphere and Climate of the Greater Bay Area, Shenzhen, China, [4]Shenzhen Key Laboratory of Precision Measurement and Early Warning Technology for Urban Environmental Health Risks, School of Environmental Science and Engineering, Southern University of Science and Technology, Shenzhen, China

Abstract Non-methane volatile organic compounds (NMVOCs) have a significant impact on air quality in urban areas. Detecting NMVOCs emission with its proxy HCHO on urban scales from space, however, has been limited by the lack of discernible enhancement. Here we show clear urban HCHO plumes from 16 cities over the globe by rotating TROPOspheric Monitoring Instrument HCHO pixels according to wind directions. We fit the downwind structure of the plumes with the exponentially modified Gaussian approach to quantify urban HCHO effective production rates between 7.0 and 88.5 mol s^{-1}. Our results are in line with total NMVOC emissions from the EDGAR inventory ($r = 0.76$). Our work offers a new measure of total NMVOC emissions from urban areas and highlights the potential of satellite HCHO data to provide new information for monitoring urban air quality.

Plain Language Summary Non-methane volatile organic compounds (NMVOCs) play an important role in urban air quality. Formaldehyde (HCHO) satellite observations have been shown to be able to reliably track and quantify NMVOC emissions at global and regional scales. Here, we use state-of-the-art satellite sensors to quantify effective HCHO production rates in 16 global cities and further constrain total NMVOC emissions. Our results are broadly consistent with current emissions inventories, implying that satellites may be able to provide new information for urban air studies.

1. Introduction

Atmospheric formaldehyde (HCHO) is an intermediate produced via primary emission and secondary formation from the oxidation of a range of volatile organic compounds (VOCs). Therefore, the production rate of HCHO provides a potential constraint on the underlying VOC emissions (Barkley et al., 2013; Bauwens et al., 2022; Shen et al., 2019; Zhu et al., 2014). Previous field measurements show that anthropogenic non-methane VOC (NMVOC) emissions are critical drivers of urban HCHO production rates (Liu et al., 2023; Zeng et al., 2019). Here, we present the first attempt to apply satellite HCHO columns to estimate effective HCHO production rates and to infer total anthropogenic NMVOC emissions in urban areas over the globe by analyzing the downwind structures of their HCHO plumes.

Regional and local HCHO enhancements are due to NMVOCs emitted by plants (Barkley et al., 2013; Millet et al., 2006; Palmer et al., 2003; Wells et al., 2020; Wolfe et al., 2016), fires (Alvarado et al., 2020; Cao et al., 2018; Holzinger et al., 1999; Yokelson et al., 1999), and human activities (Bauwens et al., 2022; Pu et al., 2022; Shen et al., 2019; Sun et al., 2021; Zhu et al., 2014; Zhu, Mickley, et al., 2017). In urban areas, the use of natural gas, diesel, gasoline, and solid fuels results in direct emissions of HCHO and secondary production of HCHO from various anthropogenic NMVOCs (Alzueta & Glarborg, 2003; Clairotte et al., 2013; Green et al., 2021).

Satellites observe HCHO from space in a column manner. Previously, HCHO tropospheric columns have been used in the inversion framework to constrain NMVOC emissions from biogenic sources (Barkley et al., 2013; Millet et al., 2006, 2008; Palmer et al., 2006; Wu et al., 2023) and fires (Cao et al., 2018; Fu et al., 2007; Gonzi

et al., 2011). However, applying HCHO columns to derive anthropogenic NMVOC emissions is challenging due to the (a) high uncertainty in the a priori estimations (Huang et al., 2017; Zheng et al., 2018), (b) lack of discernible enhancement on urban scales (Zhu et al., 2014), and (c) highly nonlinear small-scale chemistry that makes using atmospheric chemistry transport models challenging (Laughner & Cohen, 2019; Valin et al., 2013).

For gases (mainly NO_2 and SO_2) emitted from point sources (e.g., megacities or power plants), the combined analysis of satellite observations and wind fields reveals the downwind decay of plumes and has been further used to estimate their lifetimes and emissions (Beirle et al., 2011; de Foy et al., 2015; Fioletov et al., 2016; Goldberg et al., 2019; Lee et al., 2022; Lu et al., 2015). However, similar observation-based approaches have long been recognized as missing for NMVOCs, which are equally important for urban air pollution (von Schneidemesser et al., 2023). In this study, we show evident downwind decay of urban plumes over the globe with the state-of-the-art TROPOspheric Monitoring Instrument (TROPOMI) instrument (Veefkind et al., 2012) and the wind rotation technique. By fitting HCHO plumes with the exponentially modified Gaussian (EMG) function, we obtain the effective HCHO production rates and lifetimes, reflecting the emission and rapid photochemical oxidation of NMVOCs.

## 2. TROPOMI HCHO Columns and Wind Rotation Approach

Onboard the Copernicus Sentinel-5 Precursor platform, TROPOMI is a nadir-viewing spectrometer launched in October 2017, which scans the whole globe within a day at a local passing time of 13:30 and a nadir resolution of 5.5×3.5 km (7×3.5 km before August 2019). It achieves a spectral resolution of 0.55 nm in the 328–359 nm band range where HCHO retrieval is performed. We use 2019–2022 TROPOMI HCHO tropospheric vertical column product (De Smedt et al., 2018), which has been thoroughly validated (Chan et al., 2020; De Smedt et al., 2018; Vigouroux et al., 2020) and used to study NMVOC emissions (Pu et al., 2022; Sun et al., 2021; Wang et al., 2022). To ensure data quality, we select level 2 pixels with quality assurance value greater than 0.5, cloud fraction less than 0.3, and solar zenith angle less than 60°.

To investigate the downwind structures of urban HCHO plumes, we associate each pixel with its wind direction and speed, sampled from the ECMWF Reanalysis v5 (ERA5) hourly data (Hersbach et al., 2020). We use the average ERA5 wind fields in the bottom 5 levels (~up to 1.0 km above sea level), following Fioletov et al. (2015). We then apply the wind rotation technique (de Foy et al., 2015; Fioletov et al., 2015; Lu et al., 2015; Pommier et al., 2013; Valin et al., 2013) to rotate each TROPOMI pixel around the city center (apparent source) according to wind direction. Figure S1 in Supporting Information S1 illustrates the schematic of such a wind rotation approach.

First proposed by Valin et al. (2013) in their study of NO_2 urban plumes, the wind rotation approach effectively redistributes satellite observations near the source along the downwind direction. After rotation, all TROPOMI pixels have a common wind direction and thus can be analyzed together, which helps us to accumulate a statistically significant TROPOMI HCHO data set while preserving the upwind-downwind characteristics of each pixel. Another advantage of wind rotation is that it makes the central source more pronounced while attenuating the signals of the surrounding sources (Fioletov et al., 2015), which is particularly helpful for the capture of HCHO urban plumes, as for HCHO the background levels are much higher and the sources are less localized than NO_2 and SO_2.

3. Observing and Fitting Urban HCHO Plume: An Example From Riyadh

Our attempt starts with Riyadh (Saudi Arabia), one of the largest cities on the Arabian Peninsula and is usually considered as an ideal place for satellite detection of urban plumes (e.g., NO_2 and CO) due to its isolated location, large emission, and frequent clear sky conditions (Beirle et al., 2011; Lama et al., 2022; Valin et al., 2013). It is also an optimal spot to observe the HCHO urban plume as it is surrounded by desert and has low biogenic VOC emissions. Figure 1a shows the 2019–2022 mean TROPOMI HCHO tropospheric columns around Riyadh with a $0.02° \times 0.02°$ (~2×2 km) resolution. The oversampling method we use is a weighted average of the satellite pixels on each grid, with weights obtained based on the overlap area of the pixels with the grid (Zhu, Jacob, et al., 2017). Wind rotation allows us to see a distinct urban HCHO plume above the regional background (Figure 1b). By integrating the two-dimensional HCHO plume (Figure 1b) along the cross-wind direction, we obtain the one-dimensional HCHO line densities, which exhibit a Gaussian shape and decay pattern (black circles
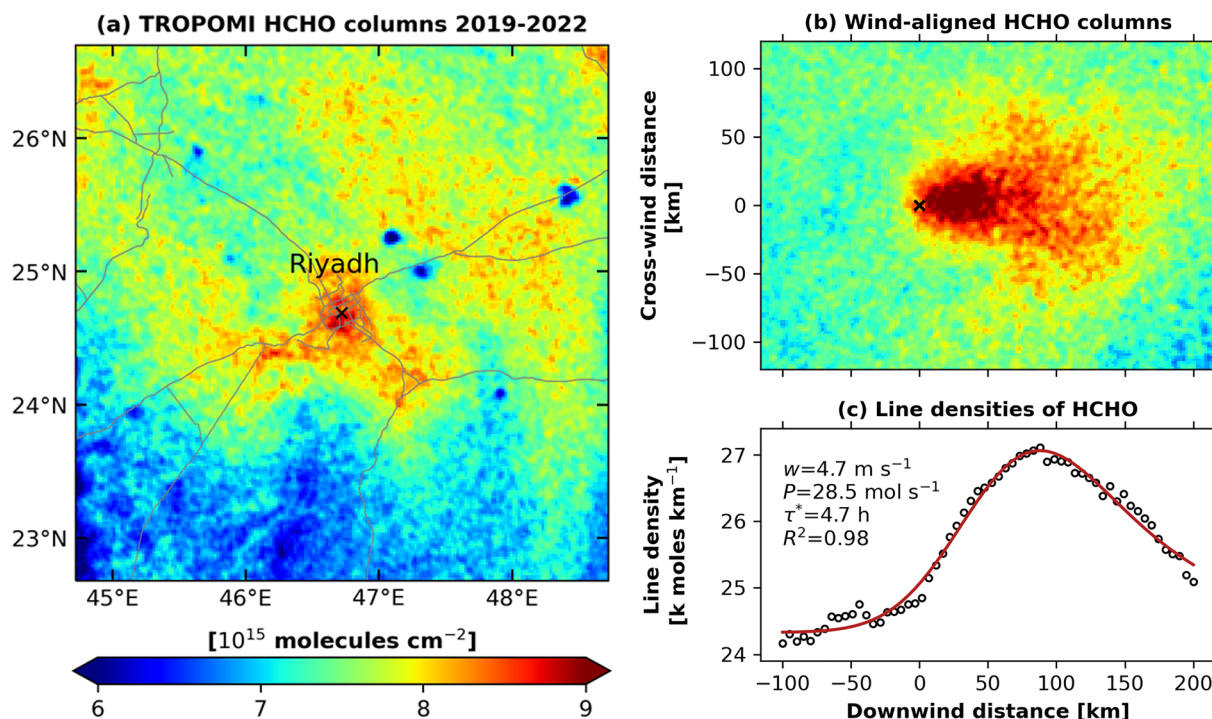
Figure 1. TROPOspheric Monitoring Instrument (TROPOMI) HCHO columns and downwind plume structure in Riyadh. (a) TROPOMI HCHO oversampled to $0.02° \times 0.02°$ (~2 × 2 km) resolution from 2019 to 2022, with the black cross marking the city center. Gray lines denote trunk roads and motorways. (b) Wind-aligned HCHO plume in Riyadh. (c) Line densities (black circles) of HCHO columns as a function of downwind distance from the city center. Each circle represents the TROPOMI HCHO line density integrated along the cross-wind direction (±100 km). The red curve ($\Omega_{\text{line}}(x)$, see Section 3) is the exponentially modified Gaussian (EMG) fitting result, with the averaged wind speed (w) from ERA5 data, fitted effective HCHO production rate (P), fitted effective lifetime (τ^*), and fitting determination coefficient (R^2) insert.

in Figure 1c). We find that the maximum enhancement of HCHO (~27 k mol km^{-1}) occurs at about 75 km downwind of Riyadh, which is almost three times the distance of NO$_2$ maximum enhancement under fast wind conditions (Valin et al., 2013). This highlights the difference in lifetimes of HCHO and NO$_2$, which implies the additional secondary production for HCHO from NMVOCs.

The exponential modified Gaussian (EMG) method has been widely applied in fitting the downwind plumes of NO$_2$ (Goldberg et al., 2019; Jin et al., 2021; Laughner & Cohen, 2019; Lu et al., 2015; Pommier, 2023) and SO$_2$ (Beirle et al., 2014; Fioletov et al., 2015; McLinden et al., 2016). This method assumes an approximate point source elevated from the background (Fioletov et al., 2022; Lange et al., 2022), which can be tested with the signal-to-noise (SNR) ratio that compares the upwind-downwind difference with satellite signals (McLinden et al., 2016; Pommier, 2023).

$$\text{SNR} = \frac{\Omega_d - \Omega_u}{\frac{\sigma_{\Omega_d}}{\sqrt{N_d}} + \frac{\sigma_{\Omega_u}}{\sqrt{N_u}}} \tag{1}$$

where Ω_d and Ω_u is the average HCHO column in downwind and upwind regions at the same distance from the center (Figure S2 in Supporting Information S1); σ_{Ω_d}, σ_{Ω_u}, N_d, and N_u is the standard deviation and number of observations in the two regions, respectively. To ensure sufficient contrast to the background, we set an *SNR* threshold of 10.0 to determine an approximate point source for HCHO, considering the lifetime of HCHO (few hours, similar to NO$_2$ and SO$_2$), resolution of TROPOMI, and size of the sources observed in each city. For Riyadh, the *SNR* value is 15.6.

The EMG method to fit HCHO line densities $\Omega_{\text{line}}(x)$ (Figure 1c) is:

$$\Omega_{\text{line}}(x|\mu, \sigma, x_0, \alpha, B) = \alpha \cdot \left[\frac{1}{x_0} \exp\left(\frac{\mu}{x_0} + \frac{\sigma^2}{2x_0^2} - \frac{x}{x_0} \right) \Phi\left(\frac{x - \mu}{\sigma} - \frac{\sigma}{x_0} \right) \right] + B \tag{2}$$

where α (mol) is a scale factor of the total number of HCHO molecules observed near the hotspot, elevated from the background (B, mol km^1); μ (km) is the location of the point source relative to the urban center (defined as $x = 0$); x_0 (km) is the e-folding distance downwind; σ (km) is the standard deviation of the Gaussian function; and Φ is the cumulative distribution of exponential function.

Similar to studies on NO_2 and SO_2 point source emissions, we define an effective lifetime of HCHO (τ^*) as:

$$\tau^* = x_0 / w \tag{3}$$

Here τ^* (hour) represents the effective mean lifetime of HCHO within the fitting domain from an approximate point source, encapsulating the effects of primary emission, secondary production, loss, and transport. w (4.7 m s^{-1}) is the effective wind speed of the study domain according to ERA5 wind fields. Further, the effective HCHO production rate P (mol s^{-1}) is defined as:

$$P = \alpha / \tau^* \tag{4}$$

which includes both primary HCHO emitted in the city and secondary HCHO produced within the downwind plume.

For Riyadh, the fitted line densities are close to TROPOMI observations with a determination coefficient (R^2) of 0.98 (Figure 1c), an effective HCHO lifetime (τ^*) of 4.3 $\pm$ 1.1 hr (95% confidence interval), and an effective HCHO production rate (P) of 33.1 $\pm$ 3.6 mol s^{-1}. The fitted background (B) is 24.4 $\pm$ 0.1 k mol km^{-1}, corresponding to a column density of 7.3×10^{15} molecules cm^{-2} in the fitting domain, which we attribute to the oxidation of regional biogenic (e.g., isoprene) and long-lived VOCs (e.g., methane). Here, we refer to Beirle et al. (2011) and Lu et al. (2015) to quantify the uncertainties of our results (Text S1 in Supporting Information S1).

4. Downwind Structures of Urban HCHO Plumes Over the Globe

As demonstrated in Riyadh (Figures 1b and 1c), the wind rotation approach enables detection of urban HCHO plumes. Based on this, we extend our analysis globally by focusing on 55 cities or urban agglomerations with populations over 5 million and another 11 cities with visible HCHO enhancements. Table S1 in Supporting Information S1 lists those 66 cities or urban agglomerations, among which 25 satisfy the point source criterion (i.e., $SNR > 10.0$).

We then apply the EMG method for each approximate point source candidate city in a 200 km by 250 km ($\pm$100 km cross-wind, 100 km upwind, and 150 km downwind) domain. This domain size is selected to minimize interference from surrounding sources (biogenic and anthropogenic) while retaining enough satellite pixels. Following Jin et al. (2021) and Laughner and Cohen (2019), we set additional criteria to obtain reasonable EMG fitting: (a) $R^2 > 0.8$, which ensures the fitted EMG curve is close to the observations; (b) $x_0 > \sigma$, which requires emission width shorter than the e-folding distance to avoid the case that emission shape confounds with HCHO decay structure; and (c) (150 km $- \mu$)/$w > \tau^*$, which states the plume residence time should be longer than the effective HCHO lifetime to reduce EMG fitting uncertainty. Table S1 in Supporting Information S1 provides whether each criterion is valid for the approximate point source candidate cities.

Figure 2 shows downwind structures of the resulting plumes in 16 cities or urban agglomerations, with wind-aligned HCHO plumes provided in Figure S3 in Supporting Information S1. Table S2 in Supporting Information S1 summarizes the corresponding EMG fitting results. The fitted effective production rate of HCHO (P) ranges from 7.0 (Esfahan) to 88.5 mol km^{-1} (Pearl River Delta), with background (B) ranges from 22.2 to 44.2 k mol km^{-1} (6.6×10^{15} to 1.32×10^{16} molecules cm^{-2}, Table S2 in Supporting Information S1). The effective lifetime (τ^*) is between 4.0 hr (Teheran) and 17.2 (Lahore) hours.

As shown in Figure 3, our effective production rates of HCHO (P) are generally in line with local total anthropogenic NMVOC (panel a; $r = 0.76$) emissions from EDGAR (v6.1) within a 100 km radius of the city center. Within the fitting domains of the 16 cities or urban agglomerations in Figure 3, biogenic isoprene emission (MEGAN v2.1 run for 2019; Guenther et al., 2012) accounts for on average 25% of the total NMVOC emissions, arguing for an anthropogenic dominated origin of HCHO. This could be further backed up by the consistency ($r = 0.78$) between effective HCHO production rates and anthropogenic nitrogen oxides (NO_x; Figure 3b) emissions.

We acknowledge the spatial heterogeneity of biogenic NMVOC emissions over hundreds of kilometers around the city, which may introduce uncertainties to the fitting results. In addition, the temporal difference between
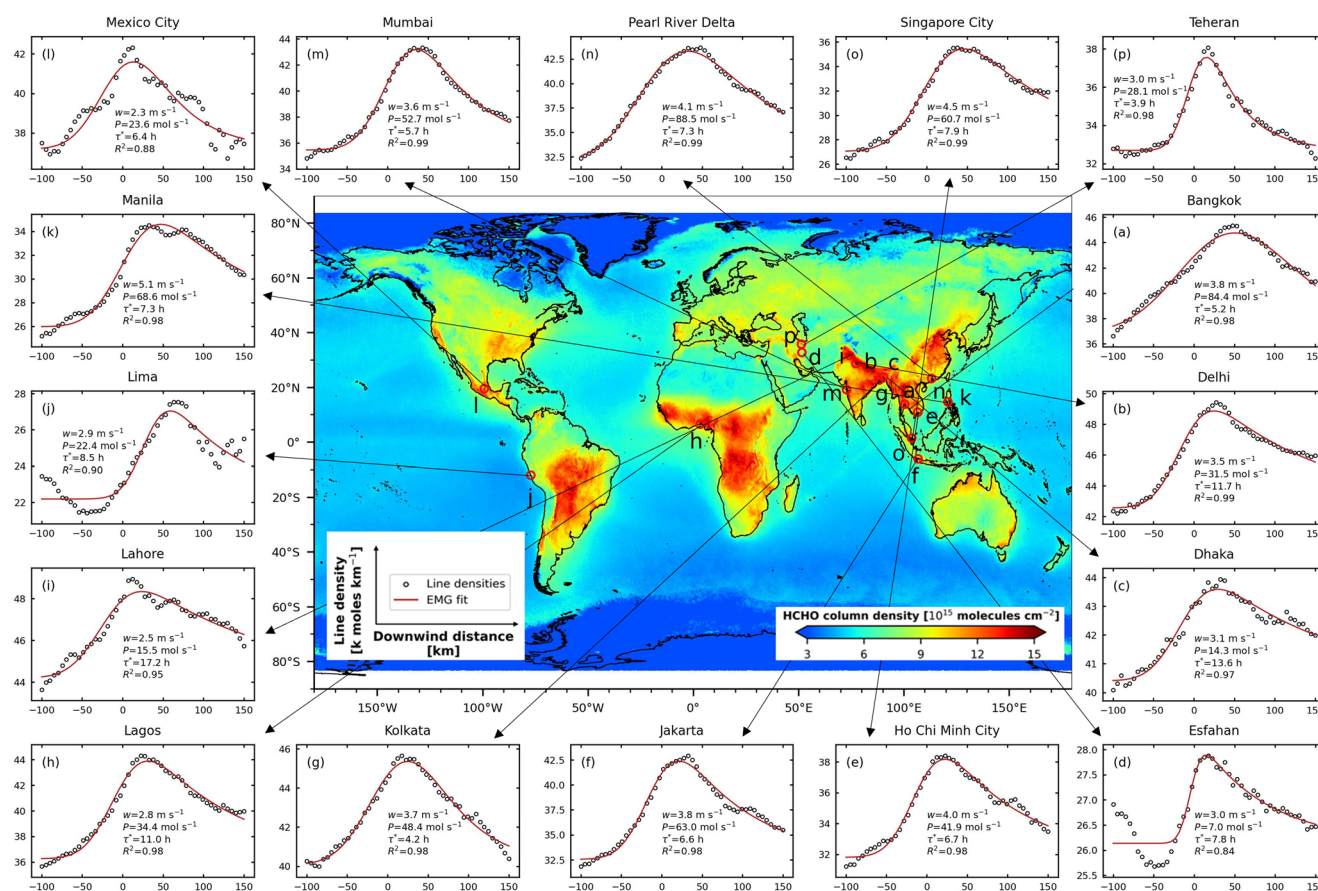
Figure 2. Global urban HCHO hotspots and their downwind plume structures. The center panel shows the mean TROPOspheric Monitoring Instrument tropospheric HCHO columns from 2019 to 2022 at a resolution of $0.1° \times 0.1°$ (~10×10 km), with HCHO hotspots circled in red. The black arrow points to the observed (black circles) and fitted (red curve) line densities for each approximate point source city (panels (a–p)). The horizontal coordinate is the downwind distance (km) from the corresponding city center. The vertical coordinate is HCHO line density (k mol km^{-1}), integrated along the cross-wind direction.
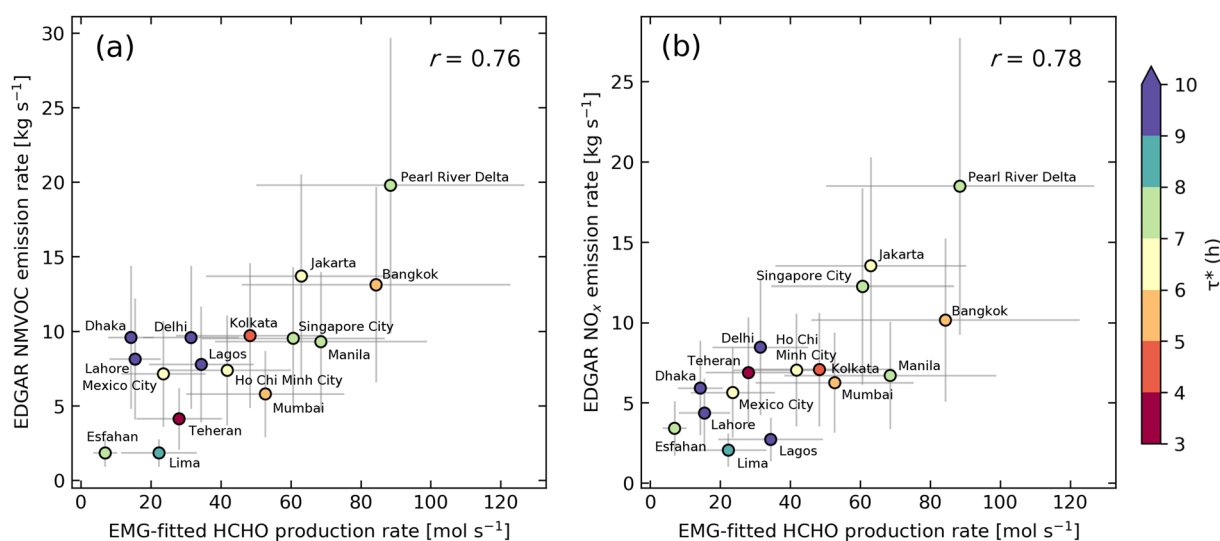
Figure 3. Comparison between EMG-fitted effective HCHO production rates with total anthropogenic Non-methane volatile organic compound (panel (a)) nitrogen oxides (NO$_x$; panel (b)) from EDGAR. The fitted rates are from the EMG fitting results (Section 4). Each point represents a city in Figure 2, colored by its fitted effective lifetime (τ^*) that saturates at 10 hr. Error bars show the total uncertainties of P_{HCHO} (Text S1 in Supporting Information S1), whereas EDGAR uncertainties are set to be 50% (Beirle et al., 2011). The Pearson correlation coefficient (r) is also inserted.

TROPOMI overpass time (13:30 local time) and EDGAR inventory (24-hr average for the year 2018) may be another source of uncertainties. Nevertheless, the broad agreement with EDGAR inventory corroborates the reliability of our approach, suggesting the effective production rate of HCHO could be a potential measure of total anthropogenic NMVOC emissions in urban areas despite NMVOCs contributing to HCHO differently under various OH levels.

Previous studies report that the EMG method accurately estimates emissions, but the effective lifetime is not a reliable measure of a gas chemical lifetime due to plume meandering and grid resolution (de Foy et al., 2015). In addition, secondary production also complicates the effective lifetime of HCHO, along with physical diffusion and chemical losses in urban plumes. That being said, τ^* depends mainly on the photolysis rate and OH concentration. If photolysis rates are known, one could determine the OH level of the urban plume (Liao et al., 2021) in a similar rationale to the study of NO_2 lifetimes (de Foy et al., 2015; Laughner & Cohen, 2019; Valin et al., 2013). Such information may help us better quantify urban atmospheric oxidation levels through satellite remote sensing.

5. Conclusion

We have used TROPOMI satellite observations and ERA5 wind fields to detect urban HCHO plumes from 16 cities over the globe. By fitting the downwind structure of the plumes, we quantify effective HCHO production rates in urban areas, which are in line with total non-methane volatile organic compound (NMVOC) emissions from the bottom-up inventory. Our work shows the potential of satellite HCHO columns in providing new information for urban air quality studies.

Data Availability Statement

We gratefully acknowledge the data set of TROPOMI HCHO product (https://doi.org/10.5270/S5P-tjlxfd2), the ERA5 data set (https://cds.climate.copernicus.eu/#!/search?text=ERA5&type=dataset), the EDGAR v4.3.2 (https://edgar.jrc.ec.europa.eu/dataset_ap432_VOC_spec), EDGAR v6.1 (https://edgar.jrc.ec.europa.eu/dataset_ap61), and the GeoNames (www.geonames.org) database. The oversampling code is available at: https://github.com/zhu-group/RegridPixels.

References

Alvarado, L. M. A., Richter, A., Vrekoussis, M., Hilboll, A., Kalisz Hedegaard, A. B., Schneising, O., & Burrows, J. P. (2020). Unexpected long-range transport of glyoxal and formaldehyde observed from the Copernicus Sentinel-5 Precursor satellite during the 2018 Canadian wildfires. *Atmospheric Chemistry and Physics*, *20*(4), 2057–2072. https://doi.org/10.5194/acp-20-2057-2020

Alzueta, M. U., & Glarborg, P. (2003). Formation and destruction of CH_2O in the exhaust system of a gas engine. *Environmental Science & Technology*, *37*(19), 4512–4516. https://doi.org/10.1021/es026144q

Barkley, M. P., Smedt, I. D., Van Roozendael, M., Kurosu, T. P., Chance, K., Arneth, A., et al. (2013). Top-down isoprene emissions over tropical South America inferred from SCIAMACHY and OMI formaldehyde columns. *Journal of Geophysical Research: Atmospheres*, *118*(12), 6849–6868. https://doi.org/10.1002/jgrd.50552

Bauwens, M., Verreyken, B., Stavrakou, T., Muller, J. F., & De Smedt, I. (2022). Spaceborne evidence for significant anthropogenic VOC trends in Asian cities over 2005-2019. *Environmental Research Letters*, *17*(1), 015008. https://doi.org/10.1088/1748-9326/ac46eb

Beirle, S., Boersma, K. F., Platt, U., Lawrence, M. G., & Wagner, T. (2011). Megacity emissions and lifetimes of nitrogen oxides probed from space. *Science*, *333*(6050), 1737–1739. https://doi.org/10.1126/science.1207824

Beirle, S., Hörmann, C., Penning de Vries, M., Dörner, S., Kern, C., & Wagner, T. (2014). Estimating the volcanic emission rate and atmospheric lifetime of SO_2 from space: A case study for Kīlauea volcano, Hawai`i. *Atmospheric Chemistry and Physics*, *14*(16), 8309–8322. https://doi.org/10.5194/acp-14-8309-2014

Cao, H. S., Fu, T. M., Zhang, L., Henze, D. K., Miller, C. C., Lerot, C., et al. (2018). Adjoint inversion of Chinese non-methane volatile organic compound emissions using space-based observations of formaldehyde and glyoxal. *Atmospheric Chemistry and Physics*, *18*(20), 15017–15046. https://doi.org/10.5194/acp-18-15017-2018

Chan, K. L., Wiegner, M., van Geffen, J., De Smedt, I., Alberti, C., Cheng, Z., et al. (2020). MAX-DOAS measurements of tropospheric NO_2 and HCHO in Munich and the comparison to OMI and TROPOMI satellite observations. *Atmospheric Measurement Techniques*, *13*(8), 4499–4520. https://doi.org/10.5194/amt-13-4499-2020

Clairotte, M., Adam, T. W., Zardini, A. A., Manfredi, U., Martini, G., Krasenbrink, A., et al. (2013). Effects of low temperature on the cold start gaseous emissions from light duty vehicles fuelled by ethanol-blended gasoline. *Applied Energy*, *102*, 44–54. https://doi.org/10.1016/j.apenergy.2012.08.010

de Foy, B., Lu, Z., Streets, D. G., Lamsal, L. N., & Duncan, B. N. (2015). Estimates of power plant NO_x emissions and lifetimes from OMI NO_2 satellite retrievals. *Atmospheric Environment*, *116*, 1–11. https://doi.org/10.1016/j.atmosenv.2015.05.056

De Smedt, I., Theys, N., Yu, H., Danckaert, T., Lerot, C., Compernolle, S., et al. (2018). Algorithm theoretical baseline for formaldehyde retrievals from S5P TROPOMI and from the QA4ECV project. *Atmospheric Measurement Techniques*, *11*(4), 2395–2426. https://doi.org/10.5194/amt-11-2395-2018

Fioletov, V. E., McLinden, C. A., Griffin, D., Krotkov, N., Liu, F., & Eskes, H. (2022). Quantifying urban, industrial, and background changes in NO_2 during the COVID-19 lockdown period based on TROPOMI satellite observations. *Atmospheric Chemistry and Physics*, *22*(6), 4201–4236. https://doi.org/10.5194/acp-22-4201-2022

Fioletov, V. E., McLinden, C. A., Krotkov, N., & Li, C. (2015). Lifetimes and emissions of SO$_2$ from point sources estimated from OMI. *Geophysical Research Letters*, *42*(6), 1969–1976. https://doi.org/10.1002/2015GL063148

Fioletov, V. E., McLinden, C. A., Krotkov, N., Li, C., Joiner, J., Theys, N., et al. (2016). A global catalogue of large SO$_2$ sources and emissions derived from the ozone monitoring instrument. *Atmospheric Chemistry and Physics*, *16*(18), 11497–11519. https://doi.org/10.5194/acp-16-11497-2016

Fu, T.-M., Jacob, D. J., Palmer, P. I., Chance, K., Wang, Y. X., Barletta, B., et al. (2007). Space-based formaldehyde measurements as constraints on volatile organic compound emissions in east and south Asia and implications for ozone. *Journal of Geophysical Research*, *112*(D6), D06312. https://doi.org/10.1029/2006jd007853

Goldberg, D. L., Lu, Z., Streets, D. G., de Foy, B., Griffin, D., McLinden, C. A., et al. (2019). Enhanced capabilities of TROPOMI NO$_2$: Estimating NO$_x$ from North American cities and power plants. *Environmental Science & Technology*, *53*(21), 12594–12601. https://doi.org/10.1021/acs.est.9b04488

Gonzi, S., Palmer, P. I., Barkley, M. P., De Smedt, I., & Van Roozendael, M. (2011). Biomass burning emission estimates inferred from satellite column measurements of HCHO: Sensitivity to co-emitted aerosol and injection height. *Geophysical Research Letters*, *38*(14), L14807. https://doi.org/10.1029/2011GL047890

Green, J. R., Fiddler, M. N., Fibiger, D. L., McDuffie, E. E., Aquino, J., Campos, T., et al. (2021). Wintertime formaldehyde: Airborne observations and source apportionment over the eastern United States. *Journal of Geophysical Research: Atmospheres*, *126*(5), e2020JD033518. https://doi.org/10.1029/2020JD033518

Guenther, A. B., Jiang, X., Heald, C. L., Sakulyanontvittaya, T., Duhl, T., Emmons, L. K., & Wang, X. (2012). The model of emissions of gases and aerosols from nature version 2.1 (MEGAN2.1): An extended and updated framework for modeling biogenic emissions. *Geoscientific Model Development*, *5*(6), 1471–1492. https://doi.org/10.5194/gmd-5-1471-2012

Hersbach, H., Bell, B., Berrisford, P., Hirahara, S., Horányi, A., Muñoz-Sabater, J., et al. (2020). The ERA5 global reanalysis. *Quarterly Journal of the Royal Meteorological Society*, *146*(730), 1999–2049. https://doi.org/10.1002/qj.3803

Holzinger, R., Warneke, C., Hansel, A., Jordan, A., Lindinger, W., Scharffe, D. H., et al. (1999). Biomass burning as a source of formaldehyde, acetaldehyde, methanol, acetone, acetonitrile, and hydrogen cyanide. *Geophysical Research Letters*, *26*(8), 1161–1164. https://doi.org/10.1029/1999GL900156

Huang, G. L., Brook, R., Crippa, M., Janssens-Maenhout, G., Schieberle, C., Dore, C., et al. (2017). Speciation of anthropogenic emissions of non-methane volatile organic compounds: A global gridded data set for 1970-2012. *Atmospheric Chemistry and Physics*, *17*(12), 7683–7701. https://doi.org/10.5194/acp-17-7683-2017

Jin, X., Zhu, Q., & Cohen, R. C. (2021). Direct estimates of biomass burning NOx emissions and lifetimes using daily observations from TROPOMI. *Atmospheric Chemistry and Physics*, *21*(20), 15569–15587. https://doi.org/10.5194/acp-21-15569-2021

Lama, S., Houweling, S., Boersma, K. F., Aben, I., Denier van der Gon, H. A. C., & Krol, M. C. (2022). Estimation of OH in urban plumes using TROPOMI-inferred NO$_2$/CO. *Atmospheric Chemistry and Physics*, *22*(24), 16053–16071. https://doi.org/10.5194/acp-22-16053-2022

Lange, K., Richter, A., & Burrows, J. P. (2022). Variability of nitrogen oxide emission fluxes and lifetimes estimated from Sentinel-5P TROPOMI observations. *Atmospheric Chemistry and Physics*, *22*(4), 2745–2767. https://doi.org/10.5194/acp-22-2745-2022

Laughner, J. L., & Cohen, R. C. (2019). Direct observation of changing NO$_x$ lifetime in North American cities. *Science*, *366*(6466), 723–727. https://doi.org/10.1126/science.aax6832

Lee, T., Wang, Y., & Sun, K. (2022). Impact of Hurricane Ida on nitrogen oxide emissions in southwestern Louisiana detected from space. *Environmental Science and Technology Letters*, *9*(10), 808–814. https://doi.org/10.1021/acs.estlett.2c00414

Liao, J., Wolfe, G. M., Hannun, R. A., St. Clair, J. M., Hanisco, T. F., Gilman, J. B., et al. (2021). Formaldehyde evolution in US wildfire plumes during the fire influence on regional to global environments and air quality experiment (FIREX-AQ). *Atmospheric Chemistry and Physics*, *21*(24), 18319–18331. https://doi.org/10.5194/acp-21-18319-2021

Liu, D., Wang, M., Hu, K., Liu, Z., Dong, H., Zhang, B., et al. (2023). Sources and budget analysis of ambient formaldehyde in the east-central area of the Yangtze River Delta region, China. *Atmospheric Environment*, *305*, 119801. https://doi.org/10.1016/j.atmosenv.2023.119801

Lu, Z., Streets, D. G., de Foy, B., Lamsal, L. N., Duncan, B. N., & Xing, J. (2015). Emissions of nitrogen oxides from US urban areas: Estimation from ozone monitoring instrument retrievals for 2005–2014. *Atmospheric Chemistry and Physics*, *15*(18), 10367–10383. https://doi.org/10.5194/acp-15-10367-2015

McLinden, C. A., Fioletov, V., Shephard, M. W., Krotkov, N., Li, C., Martin, R. V., et al. (2016). Space-based detection of missing sulfur dioxide sources of global air pollution. *Nature Geoscience*, *9*(7), 496–500. https://doi.org/10.1038/ngeo2724

Millet, D. B., Jacob, D. J., Boersma, K. F., Fu, T.-M., Kurosu, T. P., Chance, K., et al. (2008). Spatial distribution of isoprene emissions from North America derived from formaldehyde column measurements by the OMI satellite sensor. *Journal of Geophysical Research*, *113*(D2), D02307. https://doi.org/10.1029/2007JD008950

Millet, D. B., Jacob, D. J., Turquety, S., Hudman, R. C., Wu, S. L., Fried, A., et al. (2006). Formaldehyde distribution over North America: Implications for satellite retrievals of formaldehyde columns and isoprene emission. *Journal of Geophysical Research*, *111*(D24), D24S02. https://doi.org/10.1029/2005jd006853

Palmer, P. I., Abbot, D. S., Fu, T.-M., Jacob, D. J., Chance, K., Kurosu, T. P., et al. (2006). Quantifying the seasonal and interannual variability of North American isoprene emissions using satellite observations of the formaldehyde column. *Journal of Geophysical Research*, *111*(D12), D12315. https://doi.org/10.1029/2005jd006689

Palmer, P. I., Jacob, D. J., Fiore, A. M., Martin, R. V., Chance, K., & Kurosu, T. P. (2003). Mapping isoprene emissions over North America using formaldehyde column observations from space. *Journal of Geophysical Research*, *108*(D6), 4180. https://doi.org/10.1029/2002jd002153

Pommier, M. (2023). Estimations of NOx emissions, NO$_2$ lifetime and their temporal variation over three British urbanised regions in 2019 using TROPOMI NO$_2$ observations. *Environmental Sciences: Atmospheres*, *3*(2), 408–421. https://doi.org/10.1039/D2EA00086E

Pommier, M., McLinden, C. A., & Deeter, M. (2013). Relative changes in CO emissions over megacities based on observations from space. *Geophysical Research Letters*, *40*(14), 3766–3771. https://doi.org/10.1002/grl.50704

Pu, D., Zhu, L., De Smedt, I., Li, X., Sun, W., Wang, D., et al. (2022). Response of anthropogenic volatile organic compound emissions to urbanization in Asia probed with TROPOMI and VIIRS satellite observations. *Geophysical Research Letters*, *49*(18), e2022GL099470. https://doi.org/10.1029/2022GL099470

Shen, L., Jacob, D. J., Zhu, L., Zhang, Q., Zheng, B., Sulprizio, M. P., et al. (2019). The 2005–2016 trends of formaldehyde columns over China observed by satellites: Increasing anthropogenic emissions of volatile organic compounds and decreasing agricultural fire emissions. *Geophysical Research Letters*, *46*(8), 4468–4475. https://doi.org/10.1029/2019gl082172

Sun, W., Zhu, L., De Smedt, I., Bai, B., Pu, D., Chen, Y., et al. (2021). Global significant changes in formaldehyde (HCHO) columns observed from space at the early stage of the COVID-19 pandemic. *Geophysical Research Letters*, *48*(4), e020GL091265. https://doi.org/10.1029/2020GL091265

Valin, L. C., Russell, A. R., & Cohen, R. C. (2013). Variations of OH radical in an urban plume inferred from NO_2 column measurements. *Geophysical Research Letters*, *40*(9), 1856–1860. https://doi.org/10.1002/grl.50267

Veefkind, J. P., Aben, I., McMullan, K., Forster, H., de Vries, J., Otter, G., et al. (2012). TROPOMI on the ESA sentinel-5 precursor: A GMES mission for global observations of the atmospheric composition for climate, air quality and ozone layer applications. *Remote Sensing of Environment*, *120*, 70–83. https://doi.org/10.1016/j.rse.2011.09.027

Vigouroux, C., Langerock, B., Bauer Aquino, C. A., Blumenstock, T., Cheng, Z., De Mazière, M., et al. (2020). TROPOMI–Sentinel-5 Precursor formaldehyde validation using an extensive network of ground-based Fourier-transform infrared stations. *Atmospheric Measurement Techniques*, *13*(7), 3751–3767. https://doi.org/10.5194/amt-13-3751-2020

von Schneidemesser, E., McDonald, B. C., Denier van der Gon, H., Crippa, M., Guizzardi, D., Borbon, A., et al. (2023). Comparing urban anthropogenic NMVOC measurements with representation in emission inventories—A global perspective. *Journal of Geophysical Research: Atmospheres*, *128*(8), e2022JD037906. https://doi.org/10.1029/2022JD037906

Wang, Y., Yang, X., Wu, K., Mei, H., De Smedt, I., Wang, S., et al. (2022). Long-term trends of ozone and precursors from 2013 to 2020 in a megacity (Chengdu), China: Evidence of changing emissions and chemistry. *Atmospheric Research*, *278*, 106309. https://doi.org/10.1016/j.atmosres.2022.106309

Wells, K. C., Millet, D. B., Payne, V. H., Deventer, M. J., Bates, K. H., de Gouw, J. A., et al. (2020). Satellite isoprene retrievals constrain emissions and atmospheric oxidation. *Nature*, *585*(7824), 225–233. https://doi.org/10.1038/s41586-020-2664-3

Wolfe, G. M., Kaiser, J., Hanisco, T. F., Keutsch, F. N., de Gouw, J. A., Gilman, J. B., et al. (2016). Formaldehyde production from isoprene oxidation across NO_x regimes. *Atmospheric Chemistry and Physics*, *16*(4), 2597–2610. https://doi.org/10.5194/acp-16-2597-2016

Wu, Y., Huo, J., Yang, G., Wang, Y., Wang, L., Wu, S., et al. (2023). Measurement report: Production and loss of atmospheric formaldehyde at a suburban site of Shanghai in summertime. *Atmospheric Chemistry and Physics*, *23*(5), 2997–3014. https://doi.org/10.5194/acp-23-2997-2023

Yokelson, R. J., Goode, J. G., Ward, D. E., Susott, R. A., Babbitt, R. E., Wade, D. D., et al. (1999). Emissions of formaldehyde, acetic acid, methanol, and other trace gases from biomass fires in North Carolina measured by airborne Fourier transform infrared spectroscopy. *Journal of Geophysical Research*, *104*(D23), 30109–30125. https://doi.org/10.1029/1999JD900817

Zeng, P., Lyu, X., Guo, H., Cheng, H., Wang, Z., Liu, X., & Zhang, W. (2019). Spatial variation of sources and photochemistry of formaldehyde in Wuhan, Central China. *Atmospheric Environment*, *214*, 116826. https://doi.org/10.1016/j.atmosenv.2019.116826

Zheng, B., Tong, D., Li, M., Liu, F., Hong, C., Geng, G., et al. (2018). Trends in China's anthropogenic emissions since 2010 as the consequence of clean air actions. *Atmospheric Chemistry and Physics*, *18*(19), 14095–14111. https://doi.org/10.5194/acp-18-14095-2018

Zhu, L., Jacob, D. J., Keutsch, F. N., Mickley, L. J., Scheffe, R., Strum, M., et al. (2017). Formaldehyde (HCHO) as a Hazardous air pollutant: Mapping surface air concentrations from satellite and inferring cancer Risks in the United States. *Environmental Science & Technology*, *51*(10), 5650–5657. https://doi.org/10.1021/acs.est.7b01356

Zhu, L., Jacob, D. J., Mickley, L. J., Marais, E. A., Cohan, D. S., Yoshida, Y., et al. (2014). Anthropogenic emissions of highly reactive volatile organic compounds in eastern Texas inferred from oversampling of satellite (OMI) measurements of HCHO columns. *Environmental Research Letters*, *9*(11), 114004. https://doi.org/10.1088/1748-9326/9/11/114004

Zhu, L., Mickley, L. J., Jacob, D. J., Marais, E. A., Sheng, J., Hu, L., et al. (2017). Long-term (2005-2014) trends in formaldehyde (HCHO) columns across North America as seen by the OMI satellite instrument: Evidence of changing emissions of volatile organic compounds. *Geophysical Research Letters*, *44*(13), 7079–7086. https://doi.org/10.1002/2017gl073859